DOI: 10.1002/adma.200800487

Single-Crystalline $La_{0.7}Sr_{0.3}MnO_3$ Nanowires by Polymer-Template-Directed Chemical Solution Synthesis**

By *Adrián Carretero-Genevrier, Narcis Mestres,* Teresa Puig, Awatef Hassini, Judith Oró, Alberto Pomar, Felip Sandiumenge, Xavier Obradors,* and *Etienne Ferain*

One-dimensional nanostructures, such as nanowires, -belts, -rods, and -tubes, have stimulated enormous interest because of their singular properties associated with quantum confinement and low dimensionality, and their significant promise as building blocks for functional materials, devices, and systems.[1–5] The past decade has witnessed tremendous progress towards the synthesis and applications of 1D nanostructures of metals, semiconductors, and oxides. There are, however, relatively few multicomponent materials and complex oxides of which nanowires have been achieved.[2,5] One obvious reason for this is the inherent difficulty in controlling the reaction and achieving stoichiometry at the nanoscale. In the case of complex multicomponent oxides, chemical solution deposition (CSD) methods offer a precise control over stoichiometric composition, and have proven to be a highly flexible method for the fabrication of electronic oxide films and nanostructures.[6–8] When combined with template-directed synthesis, CSD represents a convenient and versatile method for generating 1D nanostructures.

Mixed-valence manganese oxides (manganites) posses a wide collection of intriguing electronic and magnetic properties.[9–12] Driven by their potential applications in diverse areas including bolometric applications,[13] magnetic recording, spintronic devices,[14] flash memory electroresistive devices,[15] and biomedical applications[16] considerable research has been devoted to the synthesis and characterization of manganites in both bulk and thin film forms.

In the last years, a strong interest has been raised on manganite-based nanostructures such as 1D nanowires and nanotubes[17–20] and 0D nanocubes and nanoparticles[16,21–22] have been reported. The delicate balance that exists between electronic, magnetic, and lattice degrees of freedom can be unbalanced in these materials at the nanoscale,[23] and thus new outstanding properties can be achieved. Hence, 1D manganite nanostructures are viewed as functional building blocks for the transport of charge and spins for the assembly of electronic, magnetic, and sensing devices. The development of facile, mild, and effective approaches for generating monodisperse, single-crystalline 1D manganite nanostructures with controllable shape and morphology remains a significant challenge. Template-directed synthesis[24] combined with CSD is viewed as one of the most straightforward and versatile ways of preparing 1D nanostructures. However, the achievement of single-crystalline nanowires has been elusive up to now.

In this Communication, we demonstrate that self-standing single crystalline $La_{0.7}Sr_{0.3}MnO_3$ (LSMO) nanowires can be successfully synthesized by template-assisted chemical solution deposition using track-etched polymer membranes of varying pore size. Even more, we prove that these nanowires exhibit a monoclinic crystallographic structure never observed so far in manganites. Nanowires were synthesized using a sol–gel-based polymer precursor route allowing a good control of the viscosity and stability of the precursor solution, which are crucial parameters for template-aided synthesis. Nanoporous track-etched polycarbonate (PC) or polyimide (PI) membranes (pore diameter of (100 ± 10) nm and pore density of $1 \cdot 10^9\,cm^{-2}$) were filled with the precursor solution by capillarity and served to restrict the manganite growth inside the 1D cylindrical nanostructures. The solution-filled templates were heated in a furnace at 800 °C for 5 h.

The size and morphology of the as-synthesized nanowires were initially examined using field-emission scanning electron microscopy (FE-SEM). Typical SEM images, as shown in Figure 1a, reveal that after the high-temperature thermal treatment, straight nanowires with uniform, homogeneous size along their axis direction are formed. The diameters of the obtained wires were in the range of (90 ± 10) nm, based on the nominal 100 nm pore sizes of the PI membranes used. Measured nanowires length attains several micrometers. SEM images obtained from randomly selected areas of the sample are very similar, indicating that the growth of monodisperse straight nanowires several micrometers long with controllable morphology is possible using polymer-template-directed growth from chemical solution deposition.

[*] Dr. N. Mestres, A. Carretero-Genevrier, Dr. T. Puig, Dr. A. Hassini,[+] Dr. J. Oró, Dr. A. Pomar, Dr. F. Sandiumenge, Prof. X. Obradors,
Institut de Ciència de Materials de Barcelona ICMAB
Consejo Superior de Investigaciones Científicas, CSIC
08193 Bellaterra, Catalonia (Spain)
E-mail: narcis.mestres@icmab.es
Dr. E. Ferain
Unité de Physique et de Chimie des Hauts Polymères
Université catholique de Louvain
Croix du Sud 1, 1348 Louvain la Neuve (Belgium)

[+] Present address: Laboratoire Génie des Matériaux et Procédés Associés EA 2664, École Polytechnique de l'Université de Nantes, 44306 Nantes, France.

[**] We acknowledge financial support from the MEC (NANOARTIS, MAT2005-02047; NANOFUNCIONA, NAN2004-09133-CO3-01, NANOSELECT and FPU), the Generalitat de Catalunya (Catalan Pla de Recerca SGR-0029 and XeRMAE), the CSIC (PIF-CANNAMUS), and the EU (HIPERCHEM, NMP4-CT2005-516858 and NESPA).

ADVANCED MATERIALS

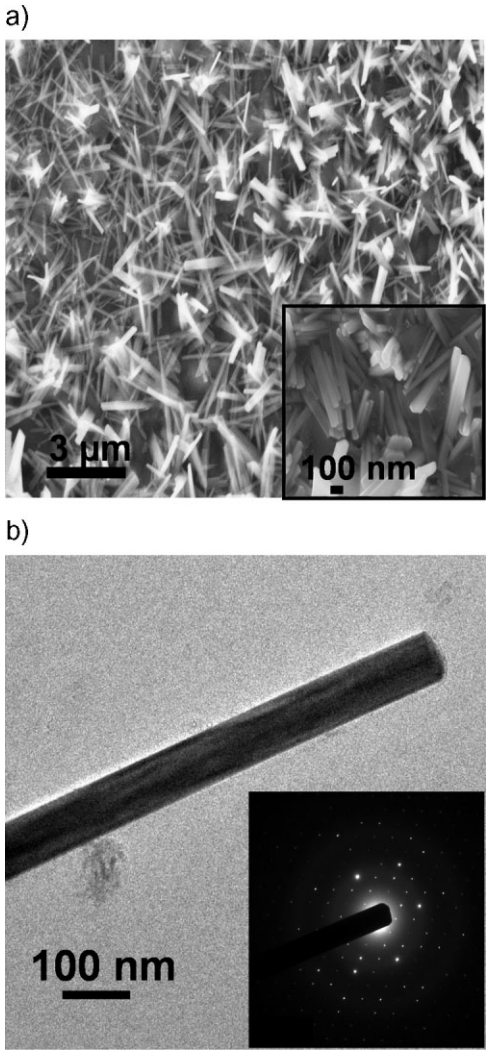

Figure 1. a) Typical FE-SEM image of LSMO nanowires prepared using polyimide membranes with 100 nm pore size. The inset shows a magnified image. b) Transmission electron microscopy image of a single LSMO nanowire. The inset shows the corresponding selected-area electron diffraction pattern.

To determine the morphology, crystallographic structure, and chemical composition of as-prepared LSMO nanostructures, individual nanowires were investigated using transmission electron microscopy (TEM). The TEM images reveal that each nanowire is uniform in width along its entire length, with smooth surfaces and diameters ranging from 80–100 nm (see Fig. 1b). The presence of sharp diffraction spots as opposed to continuous rings in the selected-area diffraction patterns (SAED) strongly supports the formation of single-crystalline LSMO nanowires. Localized chemical composition analysis by energy dispersive X-ray (EDX) spectroscopy from a number of selected regions along the nanowires confirmed that the chemical signatures associated with the synthesized compound are essentially identical within experimental accuracy and that the nanowires are composed of the elements La, Sr, and Mn. Electron energy-loss spectroscopy (EELS) line scans also showed that the nanowires are composed of La, Sr, and Mn and that the composition is uniform along the wires, with no impurities present. Furthermore, systematic SAED tilting experiments were carried out in order to investigate the crystalline structure of the nanowires. Unexpectedly, the SAED patterns along the [100], [010], and [001] zone axes (shown in Fig. 2a–c, respectively), and other planes can be indexed on the basis of a monoclinic cell with lattice parameters $a = 13.68$ Å, $b = 5.64$ Å, and $c = 21.50$ Å and $\beta = 101^\circ$. The reflection conditions (hkl) $h + k = 2n$; ($0kl$) $k = 2n$; ($h0l$) $h = 2n$; ($h0l$) $l = 2n$; ($h0l$) $l + h = 2n$, ($hk0$) $h + k = 2n$; ($h00$) $h = 2n$; ($0k0$) $k = 2n$ and ($00l$) $l = 2n$ are compatible with the monoclinic space groups $C2/c(15)$ and $Cc(9)$ according to the Joint Committee on Powder Diffraction Standards (JCPDS). Moreover, HRTEM images indicate that the nanowires long axis is along the [010] direction. In Figure 2d, a representative HRTEM image of a part of an individual LSMO nanowire along the [001] zone axis is displayed, revealing that the surfaces of the nanowires are clean, very regular, and without any sheathed amorphous phase. The distance between the parallel fringes is about 1.36 nm and 0.56 nm, corresponding to a spacing of the (100) and (010) planes of the determined monoclinic structure, respectively. The electron diffraction pattern generated by the Fourier transformation of this image (inset) shows that the LSMO nanowire is highly crystalline and is compatible with the determined monoclinic lattice. It is worthwhile to note that the unit cell volume, $V = 1628.36$ Å^3, corresponds very well to 28 times that of the pseudo-cubic unit cell of LSMO and, hence, it is evidenced that a new complex crystal lattice has been developed in these single-crystalline LSMO nanowires.

Previous studies using neutron powder diffraction have shown[25] that the structural phase diagram of $La_{1-x}Sr_xMnO_{3+\delta}$ as a function of Sr doping x and oxygen partial pressure had three structural polymorphs, that is, rhombohedral ($R\bar{3}c$), orthorhombic ($Pnma$), and monoclinic ($P2_1/c$). For doping levels $x \geq 0.18$ the rhombohedral variant $R\bar{3}c$ (pseudocubic) derived from the perovskite structure was found for the bulk form. The microstructure of $La_{0.7}Sr_{0.3}MnO_3$ films epitaxially grown by pulsed laser deposition on $LaAlO_3$ and $SrTiO_3$ (001) substrates[26] was also clarified in terms of oriented domains of the rhombohedral variant derived from the perovskite structure. Similar behavior was observed for solution deposited $La_{0.7}Sr_{0.3}MnO_3$ thin films on different single crystalline substrates.[27] However, in our case, contrary to the bulk and thin film forms, free crystallization of LSMO from chemical solution in high-aspect-ratio (1:80) preformed shapes generated in polymer templates allows to develop a new monoclinic phase which has never been observed before.

Additionally, previous works by other groups oriented to synthesize 1D manganite nanostructures using template-assisted CSD led to the formation of polycrystalline nanostructures due to the heterogeneous nucleation on the pore walls.[17–19] And when using hydrothermal synthesis[28] with no mechanical confinement present during the whole growth

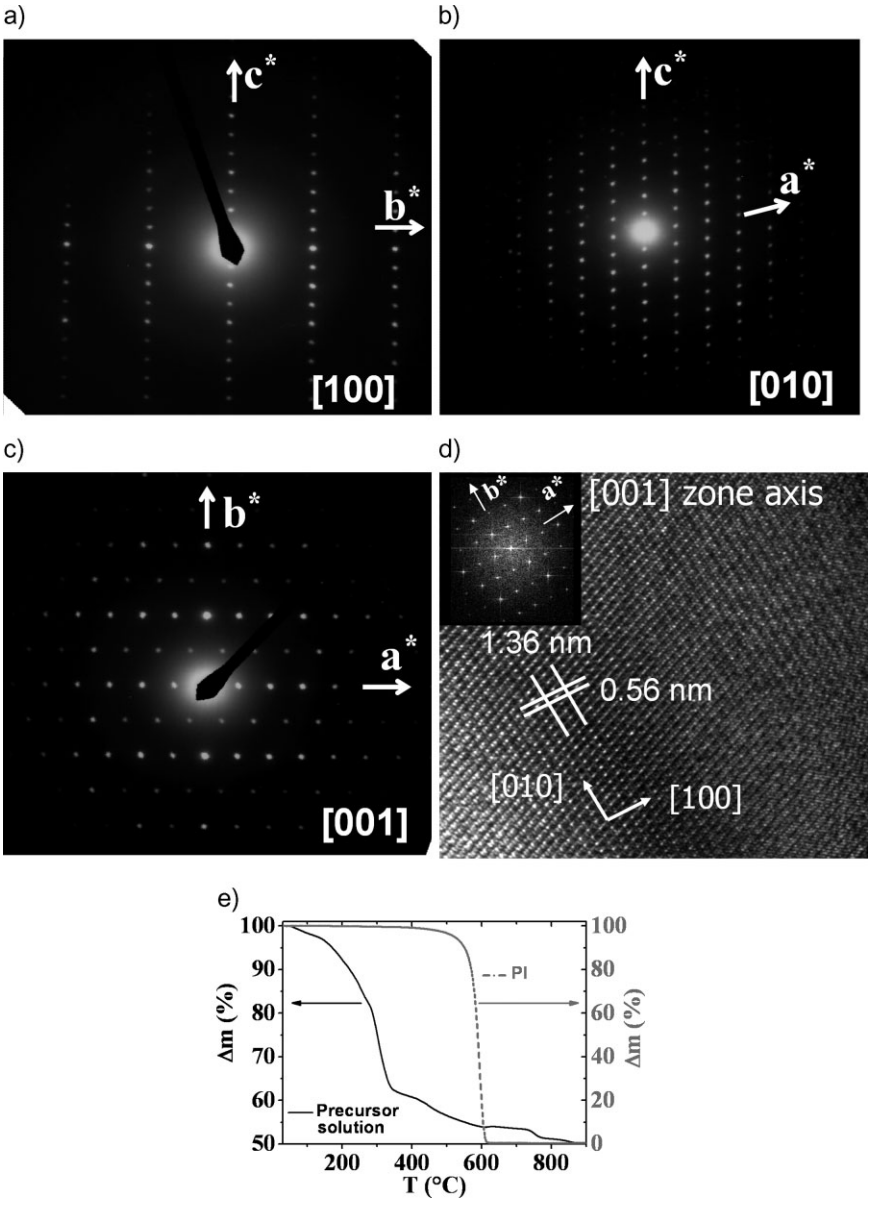

Figure 2. Electron diffraction patterns of single LSMO nanowires along the [100] (a), [010] (b), and [001] (c) zone axes. d) HRTEM image of a single LSMO nanowire along the [001] zone axis, the inset shows the Fourier transformation of this image in good agreement with the SAED pattern. e) Thermogravimetric profiles of the LSMO precursor solution and of the track-etched PI template.

process, nanowires along the ⟨110⟩ direction of the cubic perovskite structure are obtained. In contrast to these approaches, the formation of single-crystalline nanowires in our case can be attributed to the precursor solution used and to the behavior of the organic templates during the solution wetting and growth processes. In the case of a porous alumina template, confinement is present during the whole thermal cycle of the synthesis process; therefore, a strong influence of the alumina scaffold as a mechanical support and of the different thermal expansion coefficients is expected. On the contrary, when using an organic template the confinement acts only during the low temperature stages of the synthesis process, because the PI and PC templates are removed from the structures during the calcination process by combustion in the oxygen-rich atmosphere. We have corroborated this behavior by the thermogravimetric (TG) recordings of the track-etched PC and PI templates and of the precursor solution, as shown in Figure 2e. The weight loss profile of the precursor shows four different stages: The first stage of up to 160 °C is attributed to the loss of water. In the second stage up to 350 °C, a fast weight loss attributed to the PEG decomposition takes place. In a third stage from 350 to 750 °C the salts decomposition and the formation of oxides and oxycarbonates and their combination giving rise to the LSMO phase takes place. Finally, the crystallization step above 750 °C results in a small weight change. In contrast, the weight loss profile of the PI template shows its decomposition in a single step between 500 and 600 °C. This fact implies that above 600 °C once the nanopillars of oxides and oxycarbonates are already defined, the system crystallization evolves free of any mechanical confinement giving rise to a different crystallographic distortion responsible for the formation of single crystalline [010] monoclinic LSMO nanowires.

To further confirm the new crystallographic structure of the synthesized LSMO nanowires X-ray diffraction analysis with a general angle detector diffraction system (GADDS) has been performed. Figure 3a shows a typical diffraction pattern obtained from nanowires powder, the x-axis corresponds to 2θ and the rings correspond to angular direction χ, which varies with constant 2θ. The Bragg peaks of the SiO_2 support and of LSMO nanowires are identified. The θ–2θ X-ray diffraction pattern can be extracted from integrating the original 2D pattern in χ. The resulting spectrum is displayed in Figure 3b. Peak fitting performed with the FullProf routine using a profile matching model and considering the monoclinic cell obtained from the electron diffraction data, gives a very good agreement of the position of the experimental and calculated diffraction peaks. Very likely the new monoclinic structure is the most stable one at the nanometer scale. One may wonder if this structure is easily transformed to higher-symmetry structures at larger dimensions or under environmentally perturbed growth conditions.

ADVANCED MATERIALS

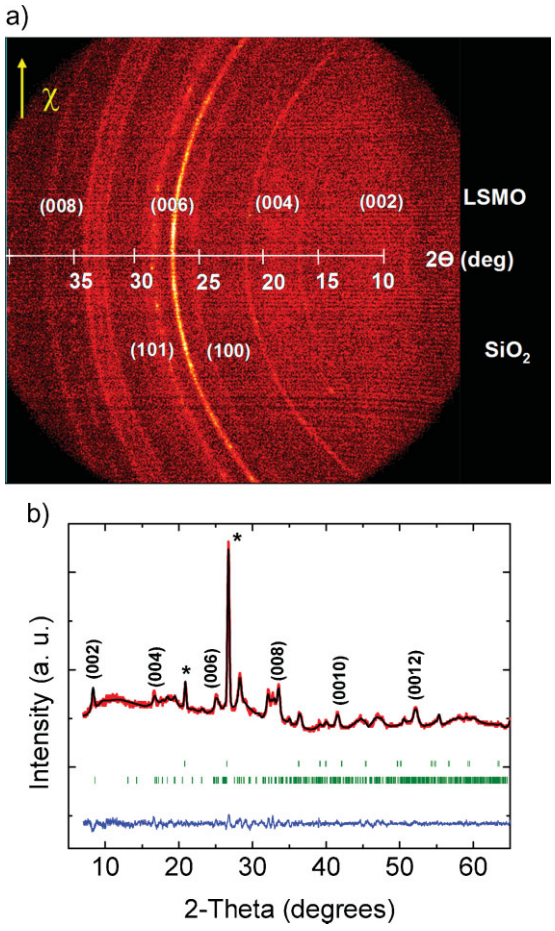

Figure 3. a) X-ray diffracted intensity recorded for single crystalline LSMO nanowires by a two dimensional GADDS detector. b) Profile matching refinement of the X-ray diffraction pattern of single crystalline nanowires on silicon substrate. Experimental data: red points; calculated: continuous black line; allowed Bragg reflections: vertical green marks. The difference between the observed and calculated profiles is displayed at the bottom (blue line).

Next we analyze the magnetic properties of the monoclinic LSMO nanowires. For this purpose, magnetic hysteresis loops were measured at different temperatures between 10 and 300 K for fields up to 5 T, with the magnetic field applied in-plane and out-of-plane with respect to the substrate where the nanowires lie. The nanowires lie mainly parallel to the substrate having a random azimuthal distribution of the long axis. Therefore, when the in-plane configuration is used the magnetic field has a random distribution with the long axis of the nanowires, while in the out-of-plane configuration the magnetic field is always approximately perpendicular to the long axis of the nanowires. Figure 4a and c displays the magnetization curves measured at 10 K and 300 K while Figure 4b and d displays magnified images of the central part of the hysteresis loops. As can be observed, they show a ferromagnetic behavior at room temperature. Moreover, Figure 4 shows that the in-plane magnetization curve leads to a saturated magnetization at smaller magnetic field than the out-of-plane curve, indicating that the direction perpendicular to the long axis of the nanowires is the hard magnetization axis.

The magnetization curves of nanowires are determined by both the intrinsic magnetocrystalline anisotropy E_{cr} and the shape anisotropy E_{sh}. Very often, in soft magnetic materials, however, shape anisotropy is dominant in high aspect ratio nanowires. In that case the anisotropy field, that is, the magnetic field required to saturate the magnetization along the hard axis direction, can be written, assuming that Stoner–Wohlfarth theory is valid,[29] as $\mu_o H_K = (2K)/M_s$, where K is the magnetic anisotropy constant. The shape contribution of nanowires to K can be easily estimated due to the large aspect ratio:

$$K_{sh} = \mu_o(1 - 3N)M_s^2/4 \quad (1)$$

where N is the demagnetizing factor ($N \sim 0$ for high aspect ratio nanowires[30]). Therefore the anisotropy field can be written as: $\mu_o H_K = 2K/M_s = \mu_o M_s/2 + 2K_{cr}/M_s$, where K_{cr} is the magneto-crystalline contribution to the magnetic anisotropy energy.

Figure 4a shows that at 10 K $\mu_o H_K \sim 0.9$ T, therefore we can estimate if this value would be consistent with a magnetic anisotropy of the nanowires fully arising from shape anisotropy. Taking into account that in LSMO at most we have $\mu_o M_s \sim 0.7$ T,[31] we must conclude that the crystalline anisotropy contribution to the magnetocrystalline field is rather high, that is, $2K_{cr}/M_s \sim 0.55$ T. If we assume that $M_s(0)$ is not modified in the present LSMO nanowires, as expected taking into account the nanowire diameter,[32] we can estimate that at $T = 10$ K, $K_{cr} \sim 15.4 \times 10^4$ J m^{-3}, which is one order of magnitude larger than the magnetocrystalline anisotropy value measured in bulk LSMO at ca. 100 K (ca. 0.9×10^4 J m^{-3})[12] but similar to that proposed for sub-micrometer particles.[33] The enhanced magnetic anisotropy is very likely associated either to a decrease of the local crystalline symmetry of Mn^{3+} ions in the new monoclinic structure, which would increase the single-ion contribution to the magnetic anisotropy,[34] or to surface effects.

Typically, magnetic remanence of strongly anisotropic nanowires along the easy magnetic axis corresponds to $M_r \sim 0.7$–0.8 M_s, while it is very small ($M_r \sim 0.05$ M_s) along the hard axes.[35] In the present case, the observation of a very small magnetic remanence ($M_r < 0.2$ M_s at 10 K) for both magnetic field orientations (see Fig. 4b) is consistent with our interpretation that the direction perpendicular to the nanowires is a hard axis. Actually, a very low fraction of nanowires strongly aligned with the magnetic field is expected for both magnetic field orientations. Similarly, the coercive field appears to be very close for both magnetic field orientations, thus indicating that it is dominated by the magnetization reversal of the hard-axis-oriented nanowires.

In summary, chemical solution deposition using a nitrates-based precursor solution with ethylene glycol as additive and assisted by track-etched polymer templates has been proven to

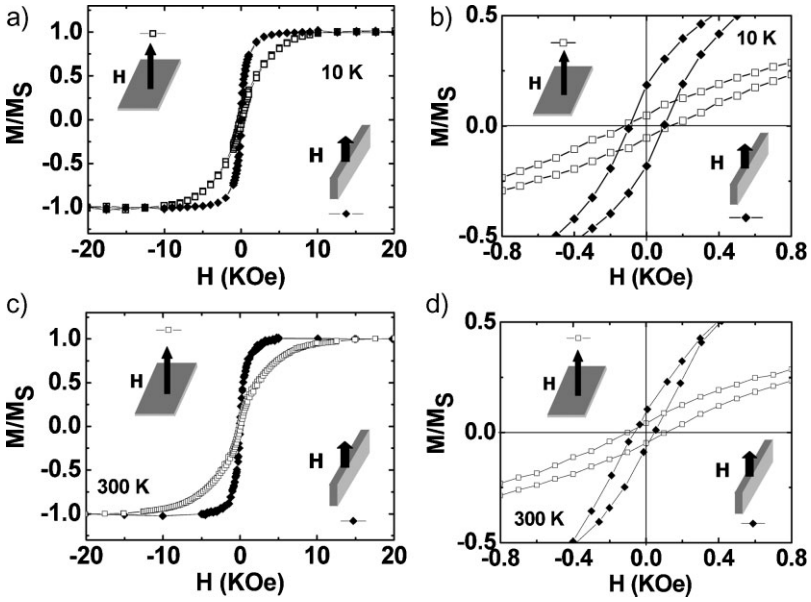

Figure 4. a) Hysteresis loops of the LSMO nanowires measured at 10 K for fields applied parallel (filled symbols) and perpendicular (open symbols) to the substrate plane. b) Low-field enlargement of the hysteresis loops measured at 10 K. c) Hysteresis loops of the LSMO nanowires measured at 300 K. d) Low-field enlargement of the hysteresis loops measured at 300 K.

be an efficient way to prepare single crystalline $La_{0.7}Sr_{0.3}MnO_3$ nanowires. The diameter of these nanowires is about 95 nm, while the length can be several micrometers. Their composition and microstructure were analyzed using X-ray diffraction, SEM, TEM, and EELS. TEM and X-ray diffraction analysis show that owing to confined growth in high-aspect-ratio nanometric pores during the initial growth stages, the nanowires crystallize in a novel monoclinic phase with the nanowire long axis along the [010] direction. The nanowires exhibit ferromagnetic ordering at room temperature and further investigations are necessary to determine if new physical properties may derive from the new crystalline structure. This methodology can be extended to other complex oxides to investigate new crystallographic phases and the modification of their physical properties.

Experimental

Sample Preparation: The LSMO precursor solution was prepared using high purity (>99.99%) metal salts $La(NO_3)_3{\cdot\cdot}6H_2O$, $Sr(NO_3)_2{\cdot\cdot}4H_2O$ and $Mn(NO_3)_2{\cdot\cdot}4H_2O$. Water used in the solution preparation was purified using the Milli-Q water treatment system. An aqueous solution of nitrates of lanthanum, manganese, and strontium in their stoichiometric ratio for $La_{0.7}Sr_{0.3}MnO_3$ was prepared, ethylene glycol was added with continuous stirring, and the whole solution was heated on a hot plate, the temperature of which was increased gradually to 150 °C. In this way, the polymerized ethylene glycol assists in forming a close network of cations and helps the reaction enabling the phase formation at low temperatures. The concentration of the final solution was adjusted to 0.9 M and the viscosity values to $\eta = 30$ mPa s. The chemical composition of the final solution was investigated by inductively coupled plasma–atomic emission spectrometry analysis on a Thermo Elemental Intrepid II XLS (Franklyn, MA, USA) spectrometer.

Nanoporous track-etched polycarbonate (PC) or polyimide (PI) membranes were produced by irradiation of the polymer film with energetic heavy ions to create tracks all across the film, followed by a preferential chemical etching to reveal tracks into pores. Irradiations were carried out with 220 MeV Ar or 420 MeV Xe ions accelerated using a cyclotron (Cyclotron Research Center, Louvain-la-Neuve, Belgium and GANIL, Caen, France) and a specific equipment dedicated to the continuous irradiation of polymer film. For these experiments, 10 μm thick PC and 7 μm thick PI irradiated films were etched to reach a pore diameter of (100 ± 10) nm at a pore density of 1×10^9 cm^{-2}; precise characterization of pore size and pore density was therefore performed using field-emission electron microscopy (LEO985). The track-etched polymer templates were filled with the precursor solution by capillarity, and after carefully wiping both template sides to remove the excess of solution and prevent the formation of a surface film, the membranes were supported on top of a clean polished silicon substrate to have mechanical stability. Finally, annealing was performed at 800 °C for 5 h in an oxygen-controlled atmosphere.

Sample Characterizations: Field-emission electron microscopy (LEO 1530) was used to characterize the morphology and size of the as synthesized samples. X-ray diffraction measurements were carried out using a Bruker AXS GADDS equipped with a 2D X-ray detector. These X-ray diffraction results were adjusted using the ''Le Bail'' fitting method, which does not require any structural information, except unit cell and resolution instrumental parameters. The refinement used here is called ''Profile Matching'' in FullProf, a program for Rietveld analysis [36]. The microstructure and local chemical composition of the samples was investigated by using a Jeol 1210 transmission electron microscope operating at 120 KV, equipped with a side-entry 60 °/30 ° double tilt Gatan 646 analytical specimen holder and a link QX2000 XEDS element analysis system. The specimens for electron microscopy were prepared by dispersion of the nanowires in methanol and deposition of a droplet of this suspension on a carbon-coated film supported on a copper grid. High-resolution electron microscopy images were obtained using a Jeol 2011 transmission electron microscope operating at 200 KV and Jeol 2010 FEG transmission electron microscope operating at 200 KV and equipped with a Gatan image filter 200 electron energy-loss spectrometer with an energy resolution of 0.8 eV. Magnetization measurements of the nanowires were made in a dc superconducting quantum interference device (SQUID) magnetometer (Quantum Design MPMS-XL7) in fields between 0 and 7 T and from 10 to 300 K, using a sample composed of a Si substrate where the LSMO nanowires were randomly distributed parallel to the substrate.

Received: February 19, 2008
Revised: April 23, 2008
Published online:

[1] Y. Xia, P. Yang, Y. Sun, Y. Wu, B. Mayers, B. Gates, Y. Yadong, F. Kim, H. Yan, *Adv. Mater.* **2003**, *15*, 353.
[2] C. N. R. Rao, F. L. Deepak, G. Gundiah, A. Govindaraj, *Prog. Solid State Chem.* **2003**, *31*, 5.
[3] H. J. Fang, P. Werner, M. Zacharias, *Small* **2006**, *2*, 700.
[4] C. M. Lieber, Z. L. Wang, *MRS Bull.* **2007**, *32*, 99.
[5] Y. Mao, T.-J. Park, F. Zhang, H. Zhou, S. S. Wong, *Small* **2007**, *3*, 1122.

ADVANCED MATERIALS

[6] R. W. Schwartz, T. Schneller, R. Waser, *C. R. Chim.* **2004**, *7*, 433.

[7] J. Gutiérrez, A. Llordés, J. Gázquez, M. Gibert, N. Romà, S. Ricart, A. Pomar, F. Sandiumenge, N. Mestres, T. Puig, X. Obradors, *Nat. Mater.* **2007**, *6*, 367.

[8] M. Gibert, T. Puig, X. Obradors, A. Benedetti, F. Sandiumenge, R. Hühne, *Adv. Mater.* **2007**, *19*, 3937.

[9] *Colossal Magnetoresistance, Charge Ordering and Related Properties of Manganese Oxides* (Eds: C. N. R. Rao, B. Raveau), World Scientific, Singapore **1998**.

[10] *Colossal Magnetoresistive Oxides*, (Ed.: Y. Tokura), Gordon and Breach, New York **1999**.

[11] M. R. Ibarra, J. M. de Teresa, P. A. Algarabel, C. Marquina, B. García-Landa, L. Morellon, C. Ritter, R. Mahendiran, A. del Moral, *Magnetostriction in Mixed Valent Magnetic Oxides,* in *Modern Trends in Magnetostriction Study and Applications*, (Ed.: M. R. J. Gibbs), Kluwer Academic Publishers, Dordrecht, The Netherlands **2000**, pp 171–204.

[12] A. M. Haghiri-Gosnet, J. P. Renard, *J. Phys. D* **2003**, *36*, R127.

[13] R. J. Choudhary, A. S. Ogale, S. R. Shinde, S. Hullavarad, S. B. Ogale, T. Venkatesan, R. N. Bathe, S. I. Patil, R. Kumar, *Appl. Phys. Lett.* **2004**, *84*, 3846.

[14] M. Bibes, A. Barthélémy, *IEEE Trans. Electron Devices* **2007**, *54*, 1003.

[15] C. Jooss, L. Wu, T. Beetz, R. F. Klie, M. Beleggia, M. A. Schofield, S. Schramm, J. Hoffmann, Y. Zhu, *Proc. Natl. Acad. Sci. USA* **2007**, *104*, 13597.

[16] K. R. Bhayani, S. N. Kale, S. Arora, R. Rajagopal, H. Mamgain, R. Kaul-Ghanekar, D. C. Kundaliya, S. D. Kulkarni, R. Pasricha, S. D. Dhole, S. B. Ogale, K. M. Paknikar, *Nanotechnology* **2007**, *18*, 345101.

[17] X. Y. Ma, H. Zhang, J. Xu, J. J. Niu, Q. Yang, J. Sha, D. R. Yang, *Chem. Phys. Lett.* **2002**, *363*, 579.

[18] a) A. G. Leyva, P. Stoliar, M. Rosenbusch, V. Lorenzo, P. Levy, C. Albonetti, M. Cavallini, F. Biscarini, H. E. Troiani, J. Curiale, R. D. Sánchez, *J. Solid State Chem.* **2004**, *177*, 3949. b) A. G. Leyva, P. Stoliar, M. Rosenbusch, P. Levy, J. Curiale, H. Troiani, R. D. Sánchez, *Phys. B* **2004**, *354*, 158. c) P. Levy, A. G. Leyva, H. E. Troiani, R. D. Sánchez, *Appl. Phys. Lett.* **2003**, *83*, 5247.

[19] a) S. Shankar, S. Kar, G. N. Subbanna, A. K. Raychaudhuri, *Appl. Phys. Lett.* **2004**, *84*, 993. b) K. S. Shankar, A. K. Raychaudhuri, *Nanotechnology* **2004**, *15*, 1312.

[20] a) C. Li, B. Lei, Z. Luo, S. Han, Z. Liu, D. Zhang, C. Zou, *Adv. Mater.* **2005**, *17*, 1548. b) B. Lei, S. Hang, C. Li, D. Zhang, Z. Liu, C. Zhou, *Nanotechnology* **2007**, *18*, 044019.

[21] D. Ruzmetov, Y. Seo, L. J. Belenky, D. M. Kim, X. L. Ke, H. P. Sun, V. Chandrasekhar, C. B. Eom, M. S. Rzchowski, X. Q. Pan, *Adv. Mater.* **2005**, *17*, 2869.

[22] J. J. Urban, Y. Lian, M. H. Jo, D. S. Wang, H. K. Park, *Nano Lett.* **2004**, *4*, 1547.

[23] S. Dong, F. Gao, Z. Q. Wang, J.-M. Liu, Z. F. Ren, *Appl. Phys. Lett.* **2007**, *90*, 082508.

[24] a) C. R. Martin, *Science* **1994**, *266*, 1961. b) C. R. Martin, *Acc. Chem. Res.* **1995**, *28*, 61. c) J. C. Hulteen, C. R. Martin, *J. Mater. Chem.* **1997**, *7*, 1075.

[25] J. F. Mitchell, D. N. Argyriou, C. D. Potter, D. G. Hinks, J. D. Jorgensen, S. D. Bader, *Phys. Rev. B* **1996**, *54*, 6172.

[26] G. Van Tendeloo, O. I. Lebedev, S. Amelinckx, *J. Magn. Magn. Mater.* **2000**, *211*, 73.

[27] G. Kartopu, M. Es-Souni, *J. Appl. Phys.* **2006**, *99*, 033501.

[28] a) D. Zhu, H. Zhu, Y. Zhang, *Appl. Phys. Lett.* **2002**, *80*, 1634. b) D. Zhu, H. Zhu, Y. Zhang, *J. Phys. Condens. Matter* **2002**, *14*, L519.

[29] E. C. Stoner, E. P. Wohlfarth, *Trans. R. Soc. London* **1948**, *240*, 599.

[30] B. D. Cullity, in: *Introduction to Magnetic Materials*, Addison-Wesley, Reading, MA **1972**.

[31] M. C. Martin, G. Shirane, Y. Endoh, K. Hirota, Y. Moritomo, Y. Tokura, *Phys. Rev. B* **1996**, *53*, 14285.

[32] L. Balcells, J. Fontcuberta, B. Martínez, X. Obradors, *Phys. Rev. B* **1998**, *58*, R14697.

[33] L. Balcells, J. Fontcuberta, B. Martínez, X. Obradors, *J. Phys. Condens. Matter* **1998**, *10*, 1883.

[34] S. Chikazumi, in: *Physics of Magnetism*, Wiley, New York **1964**.

[35] J. Qin, J. Nogués, M. Mikhaylova, A. Roig, J. S. Muñoz, M. Muhammed, *Chem. Mater.* **2005**, *17*, 1829.

[36] J. Rodriguez-Carvajal, in *FullProf: A Program for Rietveld Refinement and Pprofile Matching Analysis of Complex Powder Diffraction Patterns* (ILL, unpublished). See also: J. Rodríguez-Carvajal, in *Recent Developments of the Program FULLPROF*, in *Commission on Powder Diffraction (IUCr), Newsletter* **2001**, *26,* 12.

